Magnetic and crystallographic characterization of $Pt_3Mn_xCr_{1-x}$ by XMCD and x-ray diffraction

2009 J. Phys.: Condens. Matter 21 346003

(http://iopscience.iop.org/0953-8984/21/34/346003)

J. Phys.: Condens. Matter **21** (2009) 346003 (7pp) doi:10.1088/0953-8984/21/34/346003

Magnetic and crystallographic characterization of $Pt_3Mn_xCr_{1-x}$ by XMCD and x-ray diffraction

F Baudelet[1,2], O Mathon[3], J P Itié[1], A Polian[1], J P Kappler[4] and S Pascarelli[3]

[1] IMPMC, CNRS UMR 7590, Université Pierre et Marie Curie Paris6, 140 rue de Lourmel, 75015 Paris, France
[2] Synchrotron-SOLEIL, L'Orme des Merisiers, 91192 Gif-sur-Yvette, France
[3] ESRF, 6 rue Jules Horowitz, 38000 Grenoble, France
[4] IPCMS GEMME, 23 rue du Loess, 67037 Strasbourg, France

Received 6 April 2009, in final form 1 July 2009
Published 28 July 2009
Online at stacks.iop.org/JPhysCM/21/346003

Abstract
We have performed XMCD and diffraction measurements on the $Pt_3Mn_xCr_{1-x}$ alloy, which show that the magnetization of Pt is independently influenced by the Mn or Cr 3d orbital. We find that the magnetic moment on Pt, and its decomposition into spin and orbital components, is uniquely determined by the relative number of Mn and Cr neighbors. We then investigate the effect of pressure on the magnetization of Pt in the $Pt_3Mn_{0.5}Cr_{0.5}$ alloy. Our high pressure data enable us to conclude that at 14 GPa the spin and orbital polarization of the Pt 5d band are augmented by about 70%, with no interaction between them.

1. Introduction

Between the alloys of the ferromagnetic 3d transition metals (X) and paramagnetic 5d elements, the alloys based on platinum have attracted much attention because of their useful magnetic and electronic properties. In Pt_3Cr and Pt_3Mn the occurrence of a ferromagnetic order in compounds constituted by two elements that are normally not ferromagnetic is unusual. The induced magnetic moment of the 5d band of platinum in Pt_3Mn is found to be of pure spin origin whereas it is found to be mainly orbital in Pt_3Cr. Furthermore the third Hund's rule is violated in the Cr 3d band of Pt_3Cr because of the influence of the spin–orbit coupling on Pt [1].

This work explores the hybridization mechanism of the Pt/X d bands by Pt L_{23} x-ray magnetic circular dichroism (XMCD) measurements on $Pt_3Mn_xCr_{1-x}$ compounds using two different approaches. We first vary x to change the weight of the Cr or Mn 3d band influence on the Pt 5d band properties. We then fix the concentration at the mid-point ($x = 0.5$) and apply pressure to investigate the pressure evolution of the XMCD signal in a system where both Cr and Mn equally influence the magnetic properties. The main effect of applying hydrostatic pressure is that of decreasing bond lengths, therefore allowing tuning of the Pt/5d–X/3d band hybridization strength while monitoring the magnetic moment on Pt.

We performed x-ray diffraction (XRD) to track the onset of non-hydrostatic strain (peak broadening) and chemical disorder (strong enlargement coupled to the disappearance of the simple cubic peaks), and then to correlate these to the evolution of the magnetic properties.

Pt and 3d transition metals form binary alloys in a wide range of concentration ratios, exhibiting various magnetic properties. The concentration range for the occurrence of an fcc solid solution for Cr/Pt or Mn/Pt extends between 0 and 70% and 0 and 40%, respectively.

For stoichiometric compositions XPt and Pt_3X or PtX_3 and for transition metals from V to Ni, the crystalline phases are CuAuI-type and Cu_3Au-type, respectively [2–4].

The crystallographic properties strongly influence the magnetic and electronic properties [5]. A large variety of magnetic structures have been found in these systems, depending on the chemical ordering, the concentration of Pt and the choice of 3d element (V, Cr, Mn, Fe, Ni, Co). For Cu_3Au-type ordered alloys, ferromagnetism is found in $MnPt_3$, Fe_3Pt, $CoPt_3$ and $NiPt_3$ while $FePt_3$ is antiferromagnetic [2] and $CrPt_3$ is ferrimagnetic [6–8].

The magnetization is maximum for ordered $Pt_3Mn_xCr_{1-x}$ alloys containing 75% Pt at any x value [9]. The major magnetic moment is carried by the Mn and Cr atoms [1, 2]. A small moment is induced in the Pt atom. In Pt_3Mn, the

Pt moment is parallel to that of the Mn. In Pt_3Cr, the alignment is anti-parallel. For an intermediate concentration, the alignment of Pt is supposed to change from ferro to ferrimagnetic. Nevertheless calculations of spin density around the Pt atomic site [10] in Pt_3Cr reveal positive and negative regions, in such a way that the sign of the integrated moment could change with environmental conditions in a non-trivial way. In the disordered phase, both Pt_3Mn and Pt_3Cr alloys are paramagnetic.

XMCD measurements at the $L_{2,3}$ edges of Pt in Pt_3Cr and Pt_3Mn have been reported by Maruyama [6] and Grange [7]. Large XMCD effects at the Pt $L_{2,3}$ edges are found in Pt_3Cr and Pt_3Mn. The XMCD signal is negative at the L_3 and positive at the L_2 edge in Pt_3Mn, while it is positive at both L_3 and L_2 edges in Pt_3Cr. The positive L_3 peak confirms the presence of a large orbital magnetic moment on Pt in Pt_3Cr. Using the XMCD sum rules [11, 12], both authors find for Pt a pure spin magnetic moment in Pt_3Mn and a pure orbital one in Pt_3Cr. Even if these results suffer from the intrinsic uncertainties due to the great number of assumptions made in the sum rules derivation, they are in good agreement with theoretical calculations of XMCD Pt $L_{2,3}$ spectra and Pt magnetic moments in these systems [2, 13].

In this work we have first followed the evolution of the induced magnetic moment on Pt in $Pt_3Mn_xCr_{1-x}$ as a function of Cr/Mn relative concentration. For this we have exploited the large contrast at the L_3 edge of Pt between the XMCD spectra of Pt_3Cr and Pt_3Mn to follow the Pt magnetic moment transformation for different values of x. We have obtained an additive property of the Mn/3d and Cr/3d influence on the Pt/5d band magnetism.

2. Experimental details

Polycrystalline samples of $Pt_3Mn_xCr_{1-x}$ were synthesized by arc-melting stoichiometric amounts of pure constituents in an Ar atmosphere. Standard annealing treatments ensured the formation of an ordered Cu_3Au-type crystal structure. All the samples were crushed in small pellets and annealed for homogeneity.

X-ray absorption spectroscopy (XAS) and XMCD were recorded at the ESRF on the dispersive XAS beamline ID24. Details of the set-up are reported elsewhere [14–16]. X-ray diffraction was recorded on the DW11 beamline at LURE.

The L_3 and L_2 edges of platinum are measured separately, each of them requiring a full re-adjustment of the optics of the beamline. The circular polarization is obtained by the use of a quarter wave plate.

The XMCD are recorded by switching the applied magnetic field for a fixed beam helicity and by switching the helicity for a fixed applied magnetic field. This gives a redundant measurement, which allows for a better precision. For each edge a new high pressure cell loading was done. The lack of pressure and hydrostaticity reproducibility between the two edges prevents a quantitative comparison of the XMCD between them. The jump at the absorption edge is normalized to 1 and the same normalization factor is applied to the corresponding XMCD signal.

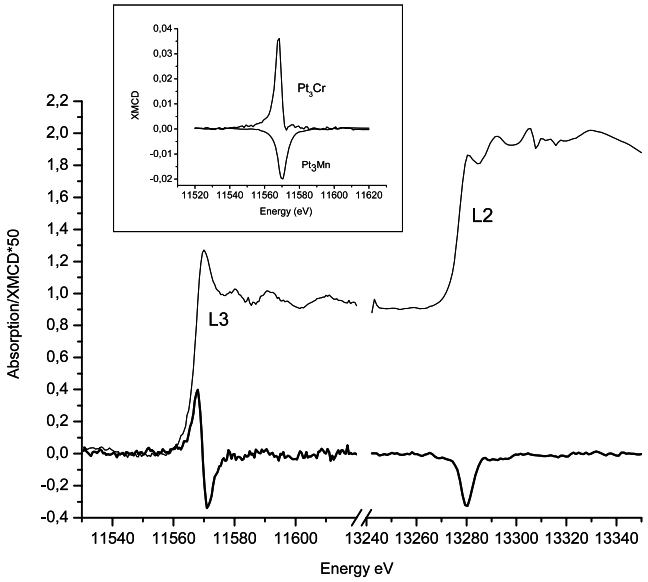

Figure 1. Absorption and XMCD signals at the $L_{2,3}$ edges of Pt on the $Pt_3Mn_{0.5}Cr_{0.5}$ sample. Inset: platinum L_3 edge XMCD signals of Pt_3Cr and Pt_3Mn: the positive peak for Pt_3Cr indicates the presence of a large orbital magnetic moment on the Pt 5d orbitals.

3. Results

3.1. XMCD

Typical absorption and XMCD signals at the $L_{2,3}$ edges of Pt on the $Pt_3Mn_{0.5}Cr_{0.5}$ sample are reported in figure 1. The L_3 XMCD signal is composed by a positive and a negative lobe whereas the L_2 signal presents one single peak. Our XMCD measurements on pure Pt_3Cr and Pt_3Mn (inset) agree with previously reported data [6, 7], namely the L_3 signals are a single negative peak for Pt_3Mn and a positive peak for the Pt_3Cr system [11, 12]. This is the signature of a spin magnetic moment on Pt in Pt_3Mn and of an orbital magnetic moment on Pt in Pt_3Cr. The Pt-site moment is coupled ferromagnetically to that on Mn and ferrimagnetically to that on Cr.

In figure 2 we report Pt L_3 edge XMCD signals measured on $Pt_3Mn_xCr_{1-x}$ for $x = 0.25$; 0.5; 0.75. We also compare our experimental data (continuous line) to a linear combination of the Pt_3Mn and Pt_3Cr XMCD spectra (symbols), with coefficients C_{Pt3Cr} and C_{Pt3Mn} given in table 1. The shape of the spectra is seen to transform progressively from a negative lobe to a positive one with Cr content, and can be reproduced by a superposition of the Pt_3Cr and Pt_3Mn spectra without any deformation. Our data are well fitted by a linear superposition of the Pt_3Cr and Pt_3Mn spectra, indicating that the magnetic moment on Pt, and its decomposition into spin and orbital components, is determined, in a first approximation, by the relative number of Cr and Mn neighbors. At the mid-point concentration ($x = 0.5$), this signal has the highest sensitivity to the Pt/5d–X/3d band hybridization strength, and for this reason, details of the shape and intensity of the signal recorded on $Pt_3Mn_{0.5}Cr_{0.5}$ samples can be used to shed more light into the hybridization mechanism.

Table 1 shows that the agreement between $(x/1-x)$ and the coefficient ratio (C_{Pt3Mn}/C_{Pt3Cr}) is very good for samples

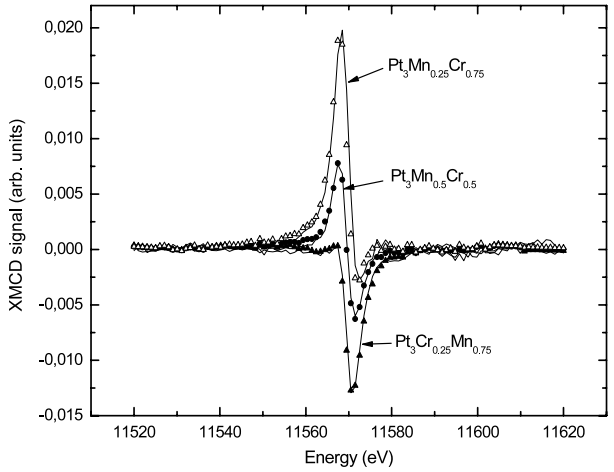

Figure 2. Pt L_3 edge XMCD signals recorded on $Pt_3Mn_xCr_{1-x}$ for $x = 0.25$, 0.5, 0.75 (continuous line) compared to interpolated signals as explained in the text (symbols). The shape of the spectra is seen to transform progressively from a Pt_3Cr-like peak to a Pt_3Mn-like one when the Mn content increases, being an exact superposition of the Pt_3Cr and Pt_3Mn spectra.

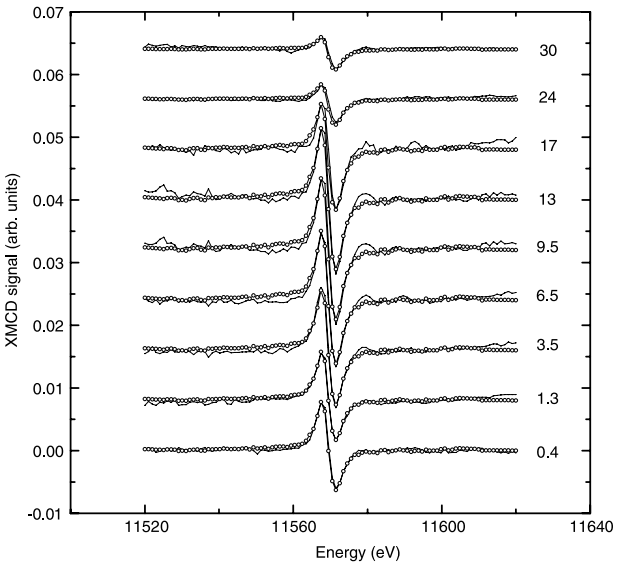

Figure 3. Pt L_3 edge XMCD signals recorded on $Pt_3Mn_{0.5}Cr_{0.5}$ for pressure between 0.4 and 30 GPa (continuous line), using ethanol/methanol/water as the pressure transmitting medium. Symbols correspond to interpolated spectra, as explained in the text.

D and E, with x equal to 0.75 and 0.25, respectively. For samples A–C ($x = 0.5$) the Mn contribution is found to be slightly stronger than for Cr because the ratio C_{Pt3Mn}/C_{Pt3Cr} is systematically higher than the concentration ratio $(x/1-x)$. This difference may be due to a direct Mn/Cr interaction. In order to clarify this point, we have, in a second step, monitored this signal as a function of pressure, i.e. as a function of interatomic Pt–Mn and Pt–Cr distances.

By acting upon the Pt–X distances, and therefore upon the Pt/5d–X/3d band hybridization strength, the net signal may either evolve maintaining the same shape (i.e. a constant balance between the Cr and Mn components), or pressure may

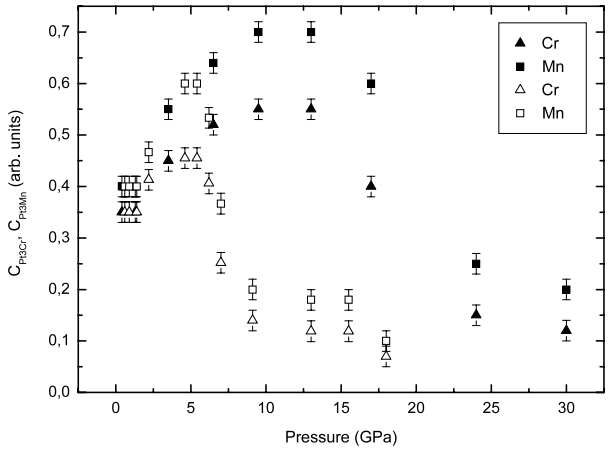

Figure 4. Decomposition of the Pt L_3 XMCD signal into Cr-like and Mn-like components for the $Pt_3Mn_{0.5}Cr_{0.5}$ compound as a function of pressure. Two sets of data are presented, corresponding to measurements with silicone oil (empty symbols) and a ethanol/methanol/water mixture (full symbols) as the pressure transmitting medium, respectively.

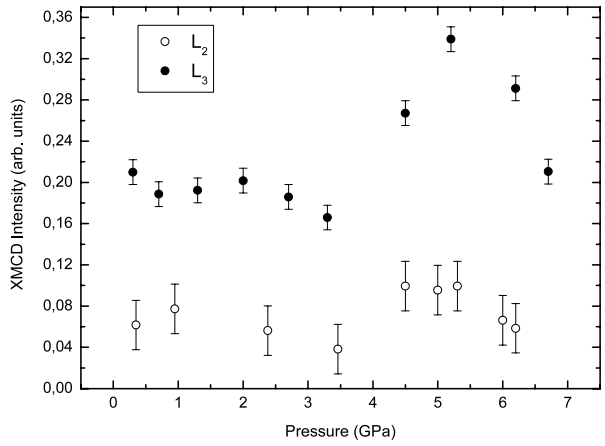

Figure 5. Pressure dependence of the XMCD signal at the Pt L edges for the pure Pt_3Cr compound.

enhance one or the other component. The shape of the signal could also evolve away from a simple linear superposition of Pt_3Mn and Pt_3Cr spectra if X–X interactions are switched on with P, which is known to lead to a paramagnetic phase.

In the following we report the results of our high pressure experiments at the Pt L_3 (figures 3 and 4) and Pt L_2 edges (figure 6) on $Pt_3Mn_{0.5}Cr_{0.5}$ as well as at the Pt $L_{2,3}$ edges on the pure compound Pt_3Cr (figure 5).

In figure 3, for each pressure point, we compare the experimental data (continuous line) to a linear combination of the ambient pressure Pt L_3 edge XMCD signals of Pt_3Cr and Pt_3Mn (symbols) and evaluate the coefficients C_{Pt3Cr} and C_{Pt3Mn}. The pressure dependence of C_{Pt3Cr} and C_{Pt3Mn} is shown in figure 4. It is interesting to note that the shape of the high pressure data is not perfectly reproduced using a linear combination of the ambient pressure Pt_3Cr and Pt_3Mn signals, in particular, between 3.5 and 17 GPa, where a small positive lobe appears around $E \sim 11\,575$ eV in the measured spectrum and cannot be reproduced.

Table 1. Best fit linear combination coefficients C_{Pt3Cr} and C_{Pt3Mn} corresponding to the Pt_3Cr and Pt_3Mn components that reproduce the Pt L_3 XMCD signals of the $Pt_3Mn_xCr_{1-x}$ samples. The three $Pt_3Mn_{0.5}Cr_{0.5}$ samples (A–C) correspond to three different sample preparations. The error bar is estimated from a large set of fits.

		$C_{Pt3Cr} \pm 0.02$	$C_{Pt3Mn} \pm 0.02$	$x/1-x \pm 0.04$	$C_{Pt3Mn}/C_{Pt3Cr} \pm 0.04$
A	$Pt_3Mn_{0.5}Cr_{0.5}$	0.50	0.60	1.0	1.2
B	$Pt_3Mn_{0.5}Cr_{0.5}$	0.50	0.60	1.0	1.2
C	$Pt_3Mn_{0.5}Cr_{0.5}$	0.35	0.40	1.0	1.14
D	$Pt_3Mn_{0.75}Cr_{0.25}$	0.25	0.75	3.0	3.0
E	$Pt_3Mn_{0.25}Cr_{0.75}$	0.60	0.20	0.3	0.3

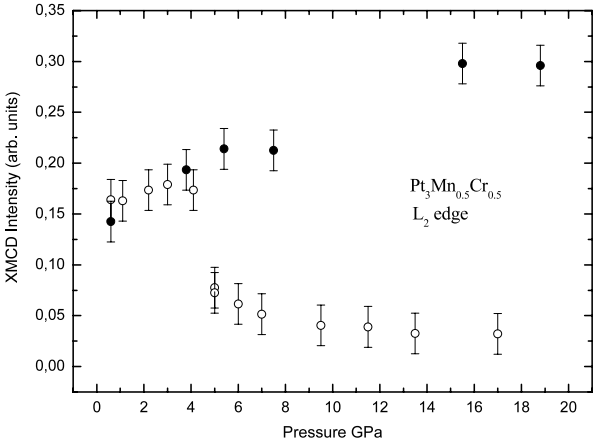

Figure 6. L_2 edge Pt XMCD signal intensity for $Pt_3Mn_{0.5}Cr_{0.5}$. Measurements with silicone oil (empty circles) and alcohol mixture (full circles) as the pressure transmitting medium, respectively.

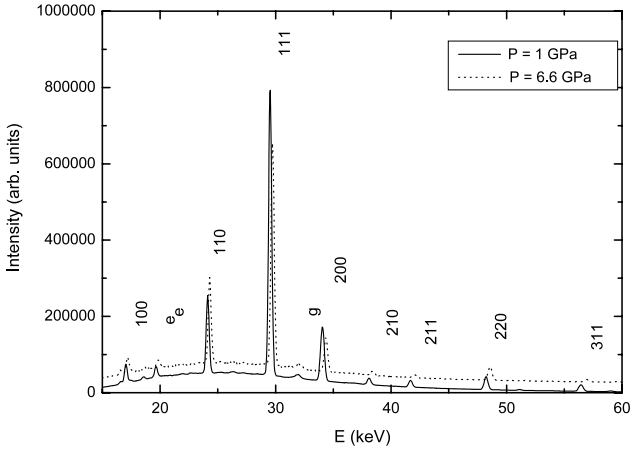

Figure 7. X-ray diffraction pattern of $Pt_3Mn_{0.5}Cr_{0.5}$ at 1 and 6.6 GPa. The peaks labeled e correspond to the escape peaks of the 111 peak. The peak labeled g corresponds to the gasket peak.

Two sets of data are presented corresponding to measurements with silicone oil (open symbols) and a 16:3:1 ethanol/methanol/water mixture (full symbols) as the pressure transmitting medium, respectively.

Both sets of values exhibit an increase of the XMCD signal under pressure up to a maximum value. The maximum is around 5 GPa and 14 GPa in silicone oil and in the water/alcohol mixture transmitting media, respectively. We will later show that these pressure values correspond to the solidification of the transmitting medium and to the loss of hydrostaticity.

The pressure dependence of C_{Pt3Cr} and C_{Pt3Mn} in silicone oil (figure 4) is somewhat similar to the XMCD signal behavior at the $L_{2,3}$ edges of Pt in the pure Pt_3Cr case (figure 5), which also shows an increase of the Pt L_3 signal, followed by a rapid decrease at the onset of solidification.

In the following, we shall refer only to the data relative to the water/alcohol mixture. Here, the increase of the signals with respect to ambient pressure is about 80% for the Mn-like part and 60% for the Cr-like part. It would be interesting to repeat the experiments in a more hydrostatic environment to follow the signal evolution at higher pressures. As shown in table 1 for the $Pt_3Mn_{0.5}Cr_{0.5}$ samples, at ambient pressure the C_{Pt3Mn} to C_{Pt3Cr} ratio shows a small excess for the Mn component. This excess increases with pressure and the relative weight C_{Pt3Mn}/C_{Pt3Cr} slightly increases from $\sim 1.2 \pm 0.04$ at ambient pressure to $\sim 1.3 \pm 0.04$ at $P = 15$ GPa.

In figure 6 we report the L_2 edge Pt XMCD signal intensity for $Pt_3Mn_{0.5}Cr_{0.5}$. Measurements with silicone oil (open symbols) and alcohol mixture (full symbols) as the pressure transmitting medium are shown. In this case it is not possible to discriminate between the 'Mn and Cr-like' contributions because they are both positive and have exactly the same shape. At the L_2 edge we also observe, for the alcohol mixture run, a signal increase at $\sim$15 GPa of about 80% with respect to ambient conditions. At this edge the signal is still high at 18 GPa, whereas at the L_3 it starts to decrease at 15 GPa. This might be due to different hydrostatic conditions due to different DAC loadings.

3.2. X-ray diffraction

X-ray diffraction has been performed on the same type of samples as those used for the XMCD measurements, i.e. small pellets, using methanol–ethanol–water mixture as a pressure transmitting medium. The experiments have been carried out in the energy dispersive mode on the DW11 wiggler beamline of DCI (LURE).

Figure 7 shows the spectra obtained in the diamond anvil cell at 1 and 6.6 GPa for $Pt_3Mn_{0.5}Cr_{0.5}$. The peaks correspond to a simple cubic structure, as expected for an ordered sample. The attribution of each peak is given in the figure.

Up to 10 GPa the intensity and the width of the peaks (figure 8) remains almost unchanged (a small variation of the relative intensities of the peaks due to a preferred orientation

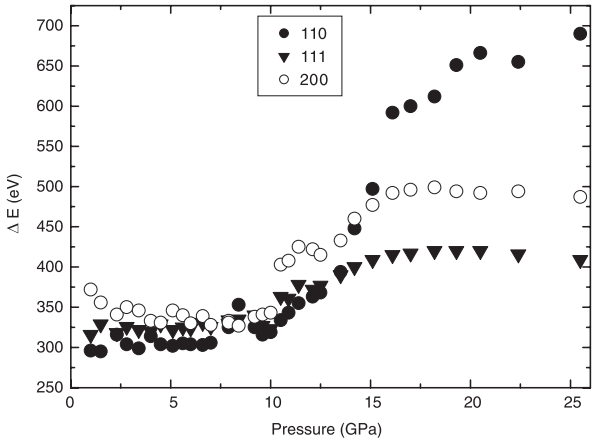

Figure 8. Variation with pressure of the width of the Bragg peaks 110 (full circles), 111 (triangles up) and 200 (empty circles).

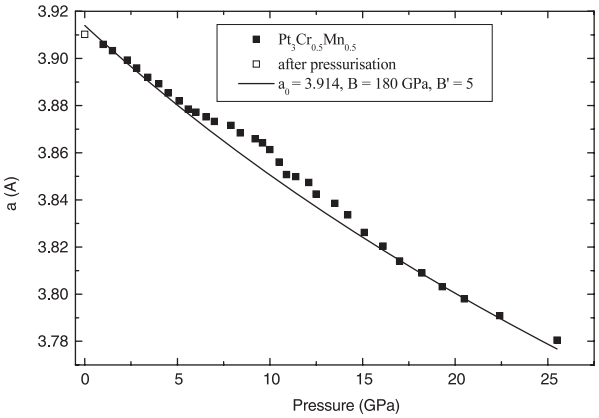

Figure 9. Lattice parameter versus pressure. Experimental (squares); the continuous line corresponds to a Birch Murnaghan equation of state with $a_0 = 3.914$, $B = 180$ GPa and $B' = 5$. a_0 is the lattice parameter at ambient pressure, B is the bulk modulus and B' its pressure derivative.

can occur for different pressures). A deviation in the compressibility occurs between 6 and 10 GPa as seen in figure 9. At 10 GPa a jump of the width of all the diffraction peaks occurs (figure 8) corresponding to the solidification of the pressure transmitting medium, while a larger decrease of the lattice parameter is observed (figure 9). At this pressure the magnetic moment on Pt is maximum and stops increasing.

Above 13.5 GPa a new increase in the width of the Bragg peaks occurs, in particular for the simple cubic peak 110. This broadening is combined with a large decrease of the intensity of the simple cubic lines. These effects suggest that the large non-hydrostatic component has started to destroy the chemical order. Chemical disorder, as expected, is also concomitant with a large decrease of the total magnetic moment. Above 20 GPa the sample becomes almost nonmagnetic and the unit cell parameter follows a normal compression curve, in the continuity of the low pressure equation of state (figure 9).

4. Discussion

In ordered Pt_3X compounds, each X transition metal site is surrounded by 12 Pt sites with no direct exchange interaction with other 3d transition metal sites. The magnetic properties in these compounds are dominated by the X/3d and Pt/5d hybridization. It is no longer the case in the disordered phases where direct X–X 3d hybridization occurs. This results in a loss of ferromagnetic order and in a paramagnetic state.

Several band-theoretical approaches within the local-spin-density approximation (LSDA) have been applied to investigate the magnetic properties of Pt_3X systems [2, 10, 17]. The electronic structure of Pt_3X is characterized by a strong hybridization of the 3d (X) transition metal and 5d Pt states. The models currently used to describe this hybridization are based on the assumption that the spin moment distribution is fairly localized near the atomic site [8], and a similar argument is made for the orbital magnetic moment [17]. The 5d Pt and 3d X orbitals are localized and hybridization occurs mainly along the axis between the two atomic sites. The details of this hybridization are described in [2], where the electronic structure of Pt_3X compounds is calculated self-consistently using the local spin density approximation and the fully relativistic spin-polarized LMTO method in the atomic-sphere approximation. The Pt 5d states are split into $d_{3/2}$ and $d_{5/2}$ states due to a strong spin–orbit (SO) coupling. This SO interaction partially removes the degeneracy of the d band in the 5d systems and can lead to the presence of an important orbital moment, which is usually almost completely quenched due to the itinerant character of the d electron and the crystal field effect. For the X 3d band, the exchange field dominates the spin–orbit coupling, so that the orbital moment is very small compared to the spin moment.

These calculations also show that hybridization with the exchange split X 3d states leads to a strong polarization of Pt 5d states at the Fermi level. In Pt_3Mn the Mn 3d majority band is nearly filled up, whereas the minority one is almost empty and gives rise to a large spin magnetic moment at the Pt site. In Pt_3Cr the majority band is only partially filled and the minority one is empty. This results in the prediction of a very small spin magnetic moment at the Pt site [2, 17]. Experimentally, it is found to be close to zero [6, 7].

We have seen that in $Pt_3Mn_xCr_{1-x}$, the Pt L_3 XMCD signal can be expressed as a simple superposition of pure 'Pt–Mn' (i.e. spin-related) and pure 'Pt–Cr' (i.e. orbital moment-related) signals. The simultaneous presence in the alloy of the two different 3d metals does not seem to introduce any additional effect to the simple combination of the properties of the two parent binary alloys. This surprising result was already observed by Maruyama [18].

Our data is therefore compatible with the following interpretation: the competition between the role of Mn/3d and Cr/3d bands does not lead, as previously expected [5, 9], to a progressive Pt single magnetic moment rotation when varying x between 1 and 0, but, to the coexistence of opposite Pt spin 'Mn-induced' and Pt orbital 'Cr-induced' magnetic moments. The total Pt magnetic moment varies between two opposite values for $x = 1$ and 0, but remains on the same axis. Our data on the $Pt_3Mn_xCr_{1-x}$ alloy (figure 2) strongly suggests that the magnetization of Pt is independently influenced by the Cr or Mn 3d orbitals. This result is consistent with the theoretical picture, whereby Pt 5d and transition metal X 3d hybridization

occurs mainly along the axis between the two atomic sites. The independence of the Pt/Cr and the Pt/Mn hybridization can originate from the geometry of the Pt 5d orbitals involved in the hybridization with the X 3d orbitals [2].

The B_{1g} and B_{2g} states at the Pt site in D_{4h} symmetry hybridize with the E_g and T_{2g} state of the X site. The basis function for the B_{1g} and B_{2g} states are respectively, $d_{x^2-y^2}$ and d_{xy}. These orbitals are centered around the Pt–X bond axis and overlap mainly with the corresponding X site 3d state. There is probably almost no mixing between the Pt states hybridized with the Cr states and the Pt states hybridized with the Mn states. This geometrical picture of hybridization oriented along the interatomic axis receives strong support in the work of Lu, Barry and Klein [10], who calculated the magnetization density of various Pt_3Cr and Pd_3Cr compounds and compared the results to structure factor measurements. The spin density around the Pt site in Pt_3Cr does not present a spherical contour centered around the Pt atom, as previously calculated in their paper (see figure 5a of [10]), but small lobes centered along the Pt–Cr axis (see figure 5c of [10]). This geometry is directly calculated from the Fourier transform of some measured magnetic form factors.

We then varied the 3d/5d hybridization strength in the $Pt_3Cr_{0.5}Mn_{0.5}$ compounds by applying pressure. As shown in figure 3, the shape of the signal changes only slightly with pressure. We still find, as at ambient, that the signal can be decomposed rather well (although not perfectly) into Pt_3Mn (i.e. spin) and Pt_3Cr (i.e. orbital) components at all pressures. Moreover, we observe that the ratio between the C_{Pt3Mn} and C_{Pt3Cr} coefficients evolves slightly with pressure (figure 4), from a value close to 1 (1.2 at ambient pressure) to 1.3 at 15 GPa, to ∼2 above 15 GPa. This trend suggests that the orbital component to the total moment on Pt (induced through hybridization with the Cr 3d orbitals) is less sensitive to pressure.

An important point which needs to be clarified in this picture is 'why the Mn contribution is always found to be slightly stronger than that of Cr for samples A–C ($x = 0.5$), and why this is enhanced with pressure'.

We can propose two explanations for this:

(1) The small difference between the Mn and Cr influence at $x = 0.5$ could originate from a small direct Mn/Cr 3d orbital interaction, which is present at ambient and is enhanced with pressure. This could possibly also explain why the linear combination of the ambient pressure Pt_3Cr and Pt_3Mn signals does not perfectly reproduce the data at high pressure up to 17 GPa. However, this explanation would not be consistent with the evolution of the signals at higher pressures ($P > 17$ GPa), the shape of which is nicely reproduced.

(2) The difference between the influence of Mn and Cr is more simply related to the different strength of their respective magnetic induced polarization on the Pt 5d band. This hypothesis agrees with the observation that the increase with pressure of the Pt L_{23} XMCD signals in $Pt_3Mn_{0.5}Cr_{0.5}$ and in Pt_3Cr are similar. This similarity rejects important direct X–X interactions below 15 GPa.

In addition, the amplitude of the XMCD signals at both edges is seen to increase with pressure up to the limit of solidification of the pressure transmitting medium (∼14–15 GPa for the water/alcohol mixture). A similar increase under pressure for the L_2 and L_3 XMCD signals was also observed for the pure Pt_3Cr compound (figure 5), yielding a pressure independent L_3/L_2 XMCD ratio, and thereby a constant value for L_z/S_z. This strongly supports a non-interacting spin and orbital magnetic moments scheme. Our high pressure data enable us to conclude that at 14 GPa the spin and orbital polarization of the Pt 5d band are respectively augmented by about 80% and 60%, without any significant interaction between them. At such pressures the Pt–X (X = Cr or Mn) distance is reduced by about 2.4%. The electronic structure of the $Pt_3Cr_{0.5}Mn_{0.5}$ compounds is very stable and this important distance variation just induces large increases in the spin and orbital magnetic moments on the Pt site.

Although the relative weight of the Pt–Mn and Pt–Cr components does vary somewhat with pressure, both lead roughly to the increase by the same magnitude of their induced Pt magnetization, within the error bars. This is assumed in the first principles calculations done in [17] of the magnetic properties of various Pt_3X systems, including Pt_3Cr and Pt_3Mn, where it is found that the 'spin magnetic moment within the muffin-tin spheres are rather insensitive to slightly different choices of the sphere radius. Also, a very good agreement is found with measurements of [6].

The x-ray diffraction results show a deviation in the compressibility between 5 and 15 GPa with a maximum at 10 GPa. In this pressure range, we also observe an important increase of the magnetic moment on Pt. The slight volume expansion, which can be connected to a 'ferromagnetic inflation' of the atomic volume, can be related to a total magnetic moment increase (mainly on Cr and Mn), while the increase of the Pt magnetic moment is due both to the increase of total magnetic moment and to the increase of the overlap between the Pt 5d electrons with the Cr and Mn 3d electrons.

The total magnetic moment in this system is extremely sensitive to uniaxial stress, as demonstrated by the XMCD experiments with silicon oil as the pressure transmitting medium (figure 4). This can be explained with the onset of important direct X–X interactions, which occurs in parallel to the loss of chemical ordering, visible around 13.5 GPa with an important broadening, combined with a large decrease of the intensity of the simple cubic lines (see figure 8).

We see a two step increase in the width of the peaks, one at ∼10 GPa, and one at 13 GPa. The first one corresponds to the loss of hydrostaticity with the solidification of the pressure transmitting medium, while the second only affects the superstructure peaks (110) and therefore corresponds to the loss of chemical order.

5. Conclusion

We performed measurements on the $Pt_3Mn_xCr_{1-x}$ alloy, which show that the magnetization of Pt is independently influenced by the Mn or Cr 3d orbitals. We find that the magnetic moment on Pt, and its decomposition into spin and orbital components,

is uniquely determined by the relative number of Mn and Cr neighbors. This result is consistent with the theoretical picture, whereby Pt 5d and transition metal X 3d hybridization occurs mainly along the axis between the two atomic sites. We observe a small difference between the influence of Mn and Cr, related to the different strength of their respective magnetic induced polarization on the Pt 5d band.

We then investigate the effect of pressure on the magnetization of Pt in the $Pt_3Mn_{0.5}Cr_{0.5}$ alloy. Here we see that the Pt–Mn (i.e. spin) and Pt–Cr (i.e. orbital) components to the signal both undergo an important increase with pressure. Our high pressure data enable us to conclude that at 14 GPa the spin and orbital polarization of the Pt 5d band are augmented by about 70%, without any interaction between them.

The platinum site carries an important magnetic orbital moment induced by Cr, which does not interact with the spin magnetic moment. This is rather surprising in a 5d metal where the presence of an orbital moment usually results from a large spin–orbit coupling.

Acknowledgment

We are grateful to G Schmerber for the preparation of samples.

References

[1] Oppeneer P M *et al* 2002 *J. Magn. Magn. Mater.* **240** 371
[2] Antonov V N, Harmon B N and Yaresko A N 2001 *Phys. Rev.* B **64** 024402
[3] Franse J J M and Gerdsdorf R 1986 *Magnetic Properties of Metals-3d, 4d and 5d Elements, Alloys and Compounds* (*Landolt-Börnstein, New Series* vol 19a) ed H P J Wijn (Berlin: Springer)
[4] Booth J G 1988 *Ferromagnetic Materials* vol 4, ed E P Wohlfarth and K H J Buschow (Amsterdam: North-Holland)
[5] Jezierski A 1993 *Physica* B **190** 225
[6] Maruyama H, Matsuoka F, Kobayashi K and Yamazaki H 1995 *J. Magn. Magn. Mater.* **140–144** 43
[7] Grange W, Kappler J P, Maret M, Rogalev A and Goulon J 1999 *J. Synchrotron Radiat.* **6** 679
[8] Shirai M, Maeshima H and Suzuki N 1995 *J. Magn. Magn. Mater.* **140** 105
[9] Williams D E G and Lewis B G 1979 *Z. Metallk.* **70** 440
[10] Lu Z W, Klein B M and Chau H T 1998 *Phys. Rev.* B **58** 9252
[11] Thole B T, Carra P, Sette F and van der Laan G 1992 *Phys. Rev. Lett.* **68** 1943
[12] Carra P, Thole B T, Altarelli M and Wang X 1993 *Phys. Rev. Lett.* **70** 694
[13] Oguchi T, Iwashita K and Jo T 1997 *Physica* B **237/238** 374
[14] Pascarelli S, Mathon O and Aquilanti G 2004 *J. Alloys Compounds* **362** 33
[15] Mathon O, Baudelet F, Itié J-P, Pasternak S, Polian A and Pascarelli S 2004 *J. Synchrotron Radiat.* **11** 423
[16] Mathon O, Baudelet F, Itié J P, Polian A, d'Astuto M, Chervin J C and Pascarelli S 2004 *Phys. Rev. Lett.* **93** 255503
[17] Iwashita K, Oguchi T and Jo T 1996 *Phys. Rev.* B **54** 1159
[18] Maruyama H 1998 private communication www.spring8.or.jp/pdf/en/res_fro/97-98/P42-P44.pdf